

PAPER

Concurrent ionic migration and electronic effects at the memristive TiO_x / $\text{La}_{1/3}\text{Ca}_{2/3}\text{MnO}_{3-x}$ interface

To cite this article: W Román Acevedo *et al* 2018 *J. Phys. D: Appl. Phys.* **51** 125304

View the [article online](#) for updates and enhancements.



LIVE WEBINAR


NanoRaman: Correlated Tip-Enhanced Optical Spectroscopy and Scanning Probe Microscopy

Thursday 8 March 15.00 GMT

REGISTER NOW!

physicsworld.com

Concurrent ionic migration and electronic effects at the memristive $\text{TiO}_x/\text{La}_{1/3}\text{Ca}_{2/3}\text{MnO}_{3-x}$ interface

W Román Acevedo^{1,3,7}, C Ferreyra^{1,3,7}, M J Sánchez^{2,3} , C Acha^{3,4}, R Gay⁵ and D Rubi^{1,3,6}

¹ GIyA e INN, CNEA, Av. Gral Paz 1499 (1650), San Martín, Buenos Aires, Argentina

² Centro Atómico Bariloche and Instituto Balseiro, 8400 San Carlos de Bariloche, Río Negro, Argentina

³ Consejo Nacional de Investigaciones Científicas y Técnicas (CONICET), Godoy Cruz 2290 (1425), Buenos Aires, Argentina

⁴ Departamento de Física, FCEyN, Universidad de Buenos Aires and IFIBA-CONICET, Pab. I, Ciudad Universitaria, Buenos Aires (1428), Argentina

⁵ CIC nanoGUNE, Tolosa Hiribidea 76, 20018 Donostia-San Sebastián, Spain

⁶ Escuela de Ciencia y Tecnología, UNSAM, Campus Miguelete (1650), San Martín, Buenos Aires, Argentina

E-mail: majo@cab.cnea.gov.ar (MJS)

Received 16 November 2017, revised 16 January 2018

Accepted for publication 13 February 2018

Published 28 February 2018



Abstract

The development of reliable redox-based resistive random-access memory devices requires understanding and disentangling concurrent effects present at memristive interfaces. We report on the fabrication and electrical characterization of $\text{TiO}_x/\text{La}_{1/3}\text{Ca}_{2/3}\text{MnO}_{3-x}$ microstructured interfaces and on the modeling of their memristive behavior. We show that a careful tuning of the applied external electrical stimuli allows controlling the redox process between both layers, obtaining multilevel non-volatile resistance states. We simulate the oxygen vacancies dynamics at the interface between both oxides, and successfully reproduce the experimental electrical behavior after the inclusion of an electronic effect, related to the presence of an *n-p* diode at the interface. The formation of the diode is due to the *n*- and *p*-character of TiO_x and $\text{La}_{1/3}\text{Ca}_{2/3}\text{MnO}_{3-x}$, respectively. Our analysis indicates that oxygen vacancies migration between both layers is triggered after the diode is polarized either in forward mode or in reverse mode above breakdown. Electrical measurements at different temperatures suggest that the diode can be characterized as Zener-type. The advantages of our junctions for their implementation in RRAM devices are finally discussed.

Keywords: resistive switching, oxide interfaces, *n-p* junctions

(Some figures may appear in colour only in the online journal)

Resistance random access memory devices display a great potential to constitute the new generation of non-volatile memories. These devices are based on the so-called resistive switching effect (RS), which consists in the reversible and non-volatile change of the resistance of metal/insulator/metal stacks upon the application of electrical stress [1, 2]. This effect has been ubiquitously found for a number

of simple and complex insulating oxides and, in particular, in the case of the celebrated magnetoresistive manganese oxides known as manganites [3]. The RS mechanism in manganite-based devices has been usually related to the electrical field induced drift of oxygen vacancies (OV) to and from manganite/metal Schottky interfaces, with the interface resistance modulated by the local concentration of OV [1]. Phenomenological models that reproduce non-trivial features of the experimental observed behavior have been developed

⁷ These authors contributed equally to this work.

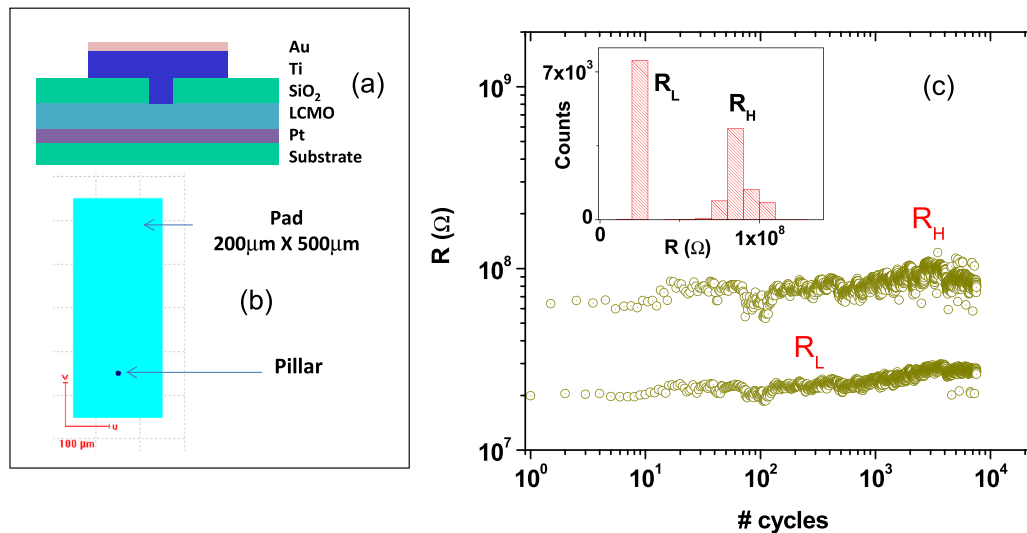


Figure 1. Sketches showing the device geometry for both cross-section (a) and top view (b); (c) bipolar resistive switching upon the application of +2 V (RESET process) and -2.5 V (SET process) pulses. Endurance was found higher than 10^4 events. The inset shows the corresponding histograms for each resistance level.

[4, 5]. Other RS mechanisms such as the formation (and disruption) of a metallic nanofilament bridging both electrodes have been observed for these devices, and in some cases a crossover between both mechanisms has been proposed [6].

Recently it was shown that when oxidizable electrodes such as Ti or Al are used, a thin oxide layer (TiO_x or AlO_x) is naturally formed at the interface between the metal electrode and the insulating oxide, and the RS behavior is related to a redox process involving the transfer of oxygen ions (vacancies) between both oxide layers [7–10]. For instance, Herpers *et al* conclusively showed by means of hard x-ray photoelectron spectroscopy that bipolar RS in $\text{Ti}/\text{Pr}_{0.48}\text{Ca}_{0.52}\text{MnO}_3$ is related to a redox process between $\text{TiO}_2/\text{Pr}_{0.48}\text{Ca}_{0.52}\text{MnO}_{3-x}$ (high resistance) and $\text{TiO}_{2-y}/\text{Pr}_{0.48}\text{Ca}_{0.52}\text{MnO}_{3-x+y}$ (low resistance) states, where oxygen transfer between both layer follows the application of electrical stimulus [7]. The formation of the TiO_x layer at the $\text{Ti}/\text{Pr}_{1-x}\text{Ca}_x\text{MnO}_3$ interface and its participation in the memristive mechanism of the interface was determined by transmission electron microscopy by Asanuma *et al*, for x ranging from 0 to 1, indicating a rather general mechanism, independent of the manganite cation stoichiometry [8]. Also, Tian *et al* [9] showed by transmission electron microscopy and its associated spectroscopic techniques that an insulating Al_xO_y layer is formed at the interface between Al and the metallic niquelate LaNiO_3 . Again, the observed RS is related to the electrical field driven exchange of OV between LaNiO_3 and the interlayer oxide, which drives a redox reaction that forms and dissolves Al nanoclusters in the Al_xO_y insulating matrix. It was also suggested in $\text{Ti}/\text{La}_{0.3}\text{Ca}_{0.7}\text{MnO}_3/\text{Si}$ systems that the oxidation and reduction of the SiO_x layer present at the $\text{La}_{0.3}\text{Ca}_{0.7}\text{MnO}_3/\text{Si}$ interface dominates the memristive behavior observed in this system [10]. We notice that the large area of these devices ($>30.000 \mu\text{m}^2$) favors the migration of Ti (top electrode material) along extended defects present in the manganite layer until a partial, non-bridging, filament is formed, inhibiting the contribution of the oxidation/reduction of interfacial TiO_x to the memristive

properties of these systems. Impedance spectroscopy experiments support the proposed scenario [10].

In this paper we report on the fabrication of $25 \mu\text{m}^2$ $\text{Ti}/\text{La}_{1/3}\text{Ca}_{2/3}\text{MnO}_3/\text{Pt}$ structures and on the study of the dynamics of OV transfer at the $\text{TiO}_x/\text{La}_{1/3}\text{Ca}_{2/3}\text{MnO}_{3-x}$ interface. The reduced dimension of these devices in comparison with those reported in [10] prevents Ti migration along extended defects and allows the redox process at the $\text{TiO}_x/\text{La}_{1/3}\text{Ca}_{2/3}\text{MnO}_{3-x}$ interface to dominate the memristive behavior. The redox process can be controlled by tuning the voltage excursion during the RESET process (low to high resistance transition) and the compliance current during the SET process (high to low transition). In this way we obtain several intermediate resistance levels, appropriate for multilevel devices. We performed numerical simulations by adapting the voltage enhanced OV drift (VEOV) model, originally developed to explain the RS behavior in single manganites samples [5, 6] and further extended for binary oxides (TiO_x) based devices [11], to include the mixed $\text{TiO}_x/\text{LCMO}_{3-x}$ scenario. We show that in addition to OV migration, an electronic effect, related to the existence of an n - p junction at the $\text{TiO}_x/\text{LCMO}_{3-x}$ interface, should be included in the modeling in order to successfully reproduce the experimental behavior.

Polycrystalline $\text{La}_{1/3}\text{Ca}_{2/3}\text{MnO}_3$ (LCMO) thin films (100 nm thick) were grown by pulsed laser deposition on top of commercial platinized silicon. Details of the growth conditions can be found on [12]. Ti top electrodes consisted in $5 \mu\text{m}$ micropillars embedded in an insulating SiO_2 matrix, and were fabricated by a combination of two steps of electronic lithography, reactive ion etching (for the SiO_2) and electron-beam deposition (for the Ti). The pillars end in rectangular macroscopic pads (suitable for making electrical contact with standard tips) covered by a thin layer of gold, to avoid Ti oxidation upon exposure to ambient conditions. Figure 1 shows a sketch with the geometry of the devices in top (a) and cross-section (b) views. Voltage-controlled electrical characterization was performed by using a Keithley 2612 source-meter

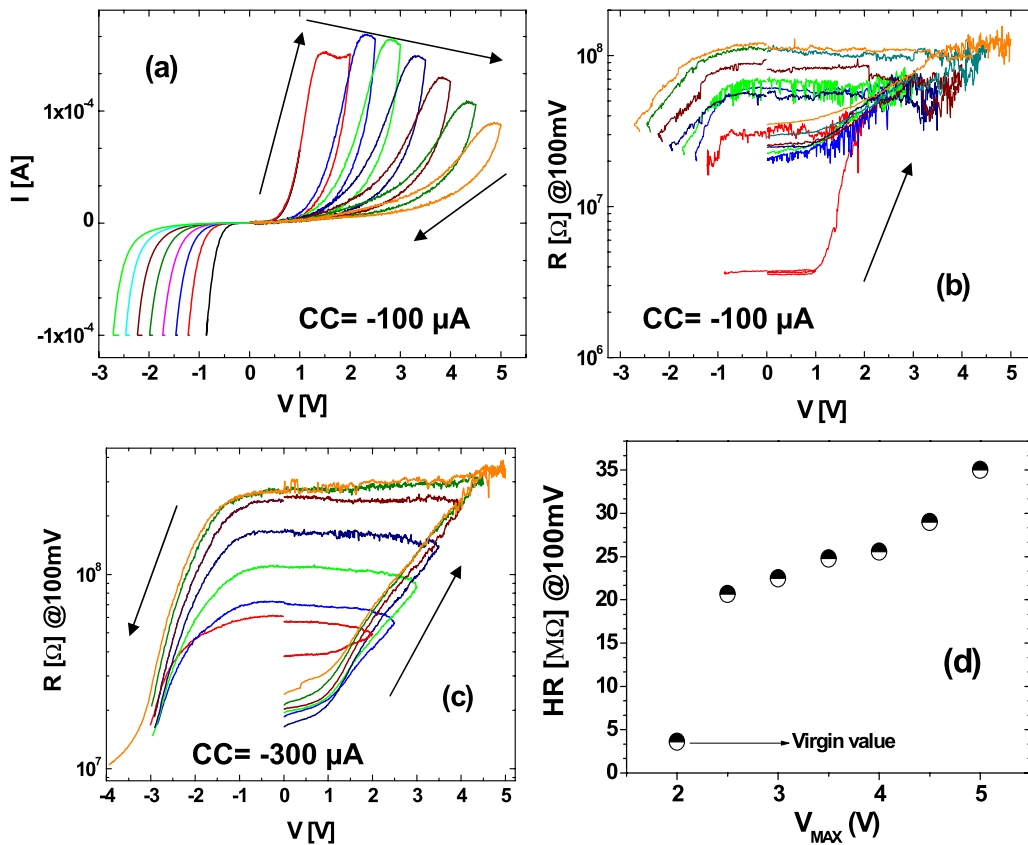


Figure 2. (a) Experimental consecutive I - V curves recorded for a $5 \mu\text{m}$ device, obtained by progressively increasing the positive voltage excursion V_{MAX} from 2.5 V to 5 V; (b) hysteresis switching loops recorded simultaneously to the I - V curves displayed in (a), with a SET $\text{CC} = -100 \mu\text{A}$; (c) hysteresis switching loops obtained after increasing the SET CC to $-300 \mu\text{A}$; (d) evolution of the (remanent) HR state for different V_{MAX} .

hooked to a commercial probe station. The Pt bottom electrode was grounded and the stimulus was applied to the top electrode. Virgin resistance values were found in the range ~ 1 – $3 \text{ M}\Omega$. Figure 1(c) shows that our devices present bipolar RS upon the application of 1 ms wide $+2 \text{ V}$ (transition from low to high resistance, RESET process) and -2.5 V (transition from high to low resistance, SET process) pulses. The endurance of the device was higher than $\sim 10^4$ cycles, and the retentivity of both resistance states was at least 24 h.

Next, we tested the electrical response of virgin devices by performing pulsed I - V curves and hysteresis switching loops (HSLs). The pulsed I - V curve is built by applying a sequence of voltage pulses of different amplitude, following the sequence $(0 \rightarrow V_{\text{MAX}} \rightarrow -V_{\text{MIN}} \rightarrow 0)$, while the current is measured during the application of the pulse. The electrical pulses were $\sim 1 \text{ ms}$ wide and were separated from each other by $\sim 1 \text{ s}$ to avoid self-heating effects. The step in the applied voltage pulses was 10 mV . After each of these pulses we apply a small reading voltage of 100 mV that allows measuring the remnant resistance state, in what is called an hysteresis switching loop.

Figures 2(a) and (b) show consecutive room temperature dynamic I - V curves and HSL obtained by progressively increasing V_{MAX} from 2.5 V to 5 V. Initially, the devices were in a low resistance state (LR) of $\sim 4 \text{ M}\Omega$. Upon the application of positive stimulus, the transition to a high resistance state (HR) occurs (RESET process). This transition is gradual and

the final HR state can be tuned by controlling V_{MAX} , from $30 \text{ M}\Omega$ to $100 \text{ M}\Omega$ (see figure 2(d)). The transition from HR to LR (SET process) is obtained with negative stimulus at a voltage $-V_{\text{SET}}$. A compliance current $\text{CC} = -100 \mu\text{A}$ is set to avoid device damage during the SET process. It is found that $-V_{\text{SET}}$ increases with the V_{MAX} of the previous cycle. We also notice that for this CC , after the SET process the LR state does not return to the value observed in the previous loop. Figure 2(c) corresponds to equivalent HSLs of figure 2(b), but with the negative compliance current set in a higher value of $-300 \mu\text{A}$. In this case, it is found that after the SET process the previous LR state is recovered. We remark that the virgin resistance value is never recovered, indicating that we can identify the first RESET event as a forming process, consistently with the work of Herpers *et al* [7]. From the latter description we remark the multilevel capability of our memory devices.

We recall that LCMO is a hole doped manganite and therefore behaves as a type p semiconductor. A thin layer close to the surface is reduced after the deposition of Ti. We refer to this layer as LCMO_{3-x} . The resistivity of this layer increases due to the presence of OV that disrupts the double exchange Mn–O–Mn bonds [13]. Additionally, the Ti layer close to the LCMO_{3-x} is partially oxidized to TiO_x , which behaves as an n -type semiconductor where the presence of OV increments its conductivity. Once the external stimulus (voltage) is applied, the OV located at the interface can be drift back and forth

between both layers, depending on the polarity of the electrical stimulus. Regarding the LCMO/Pt interface, it behaves as ohmic due to the large work function of Pt (5.6 eV) and therefore we assume that it does not contribute to the resistance changes [14]. The Ti/TiO_x interface was also assumed as ohmic, consistently with [15].

In the following we focus on the TiO_x/LCMO_{3-x} interface to analyze SET and RESET processes in terms of OV transfer. We argue that the initial configuration of OV in the pristine state (PS) is consistent with a LR state due to the non-stoichiometric TiO_x layer ($x < 2$) that contributes with a significant conductivity (see the sketch of figure 3(b)). The RESET process takes place for positive stimulus and is related to OV (positive ions) transfer from the TiO_x layer to the LCMO_{3-x} layer, the first becoming nearly stoichiometric ($x \sim 2$, highly resistive). At the same time, the OV created at the LCMO_{3-x} contribute to increase its resistance. As a consequence the HR state is associated to an OV configuration schematized in figure 3(b), second panel. Notice that the amount of transferred OV is controlled by the voltage excursion V_{MAX} . The opposite process takes place for negative stimulus and the interface returns to a LR state. However in this case, the amount of OV transferred from the LCMO_{3-x} to the TiO_x layer is controlled by the CC triggered at $-V_{SET}$ and therefore the final configuration of OV for the obtained LR state should not necessarily correspond to the initial one.

To model the described behavior we analyze the dynamics of OV across the TiO_x/LCMO_{3-x} interface. This is the active region for OV migration, that we take as a 1D chain of $N = N_L + N_R$ sites, with N_L sites corresponding to the TiO_x and N_R sites corresponding to the LCMO_{3-x}. The links are physically associated to small domains of nanoscopic dimensions in both sub-oxides, with an initial OV concentration associated to the PS. The 1D chain, although a simplification of the actual geometry, is in accordance with the experimental evidence indicating that the conduction takes place along a directional path. As the resistivity of the interface is dramatically affected by the precise oxygen stoichiometry, we characterize each site along the chain by its resistivity ρ_i , which is a function of the local OV density content δ_i . Following the previous description and taken into account that for TiO_x the resistivity decreases with the OV content, we define as in [11]

$$\rho_i^{\text{TiO}_x} = \frac{\rho_0}{1 + A_i \delta_i} \approx \rho_0 (1 - A_i \delta_i) \quad (1)$$

for the local resistivity along the first N_L sites. On the other hand we take, as in [5],

$$\rho_i^{\text{LCMO}_{3-x}} = B_i \delta_i \quad (2)$$

for the N_R sites correspondent to the LCMO_{3-x} region. This equation does not take into account the addition of a constant term related to the resistivity of the (undoped) stoichiometric LCMO, which does not affect the simulations results. The coefficients A_i 's and B_i 's are specific of each region/oxide and we take them as constants. We compute the total resistance along the interface as

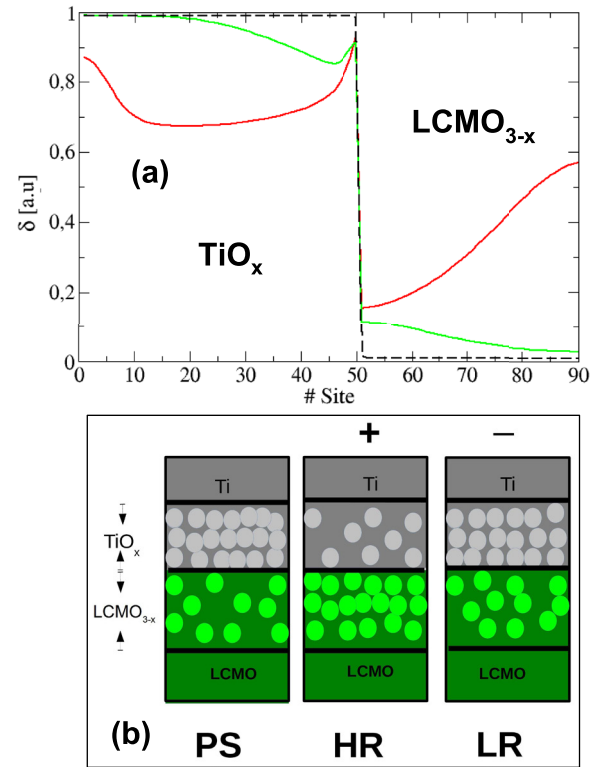


Figure 3. (a) OV profiles assumed for the pristine state (black dashed line) and obtained after running the simulations for HR (red line) and LR (green line) states; (b) sketch showing the OV distributions for both TiO_x and LCMO_{3-x} layers for pristine, HR and LR states.

$$R = C \sum_{i=1}^{N_L} \rho_i^{\text{TiO}_x} + \sum_{i=N_L+1}^N \rho_i^{\text{LCMO}_{3-x}} \quad (3)$$

with the proportionality factor taken for simplicity $C \equiv 1$. The assumed initial OV profile is shown in figure 3(a) (dashed line) and was chosen consistently with the experimental evidence reported in [7], and verified also in our samples, that the initial state is a low resistance one. This is related to the Ti layer being partially oxidized to TiO_x at expenses of a thin LCMO layer reduced to LCMO_{3-x}. This has been settled by spectroscopic characterization by the Jülich group [7]. Taking into account this initial scenario, the pristine OV density in the TiO_x should be important enough to increment the conductivity of this layer. Additionally, as the resistivity of the LCMO_{3-x} increases due to the presence of OV we need to assume an OV profile in the LCMO_{3-x} that does not destroy the LR initial state of the complete interface. The assumed initial OV profiles match these requirements. Given an external stimulus $V(t)$ (the applied voltage protocol between electrodes), the OV density profile at site i is updated at each simulation step according to the following rate probability for transfer from site i to a nearest neighbor $j = i \pm 1$, i.e.

$$p_{ij} = \delta_i (1 - \delta_j) \exp(-V_\alpha + \Delta V_i), \quad (4)$$

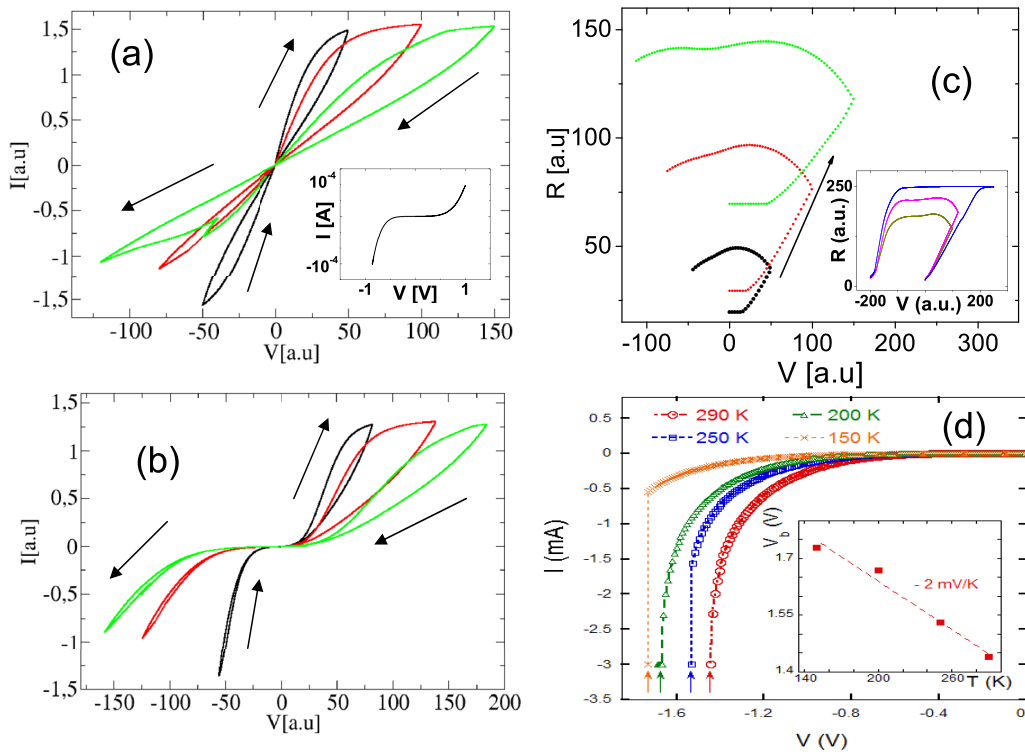


Figure 4. (a), (b) Simulated I - V curves for different voltage excursions by using the VEOV drift model, before and after including the electronic effect at the $\text{TiO}_x/\text{LCMO}_{3-x}$ interface; (c) the main panel shows the simulated HSLs associated to figure 4(b). The inset displays HSLs for a higher voltage excursion that emulates a higher experimental CC; (d) experimental I - V curves at different temperatures measured in the negative quadrant. The inset displays the evolution of the breakdown voltage V_b with T .

which is proportional to the density of vacancies present at site i , and to the available concentration at the neighbor domain j . In the Arrhenius factor, $\exp(-V_\alpha + \Delta V_i)$, the local potential drop (or local electric field) at site i , is

$$\Delta V_i(t) = V_{i+1}(t) - V_i(t) = V(t) \rho_i / R. \quad (5)$$

In addition, V_α is the activation energy for vacancy diffusion in the absence of the external applied voltage and in equation (4) all the energy scales are taken in units of $k_B T$. We consider $V_\alpha = V_0$, for sites in the chain belonging to TiO_x , and $V_\alpha = V_1$ for those sites belonging to the LCMO_{3-x} . The numerical implementation follows as in [5, 11]. We take the following parameters values: $N = 90$, $N_L = 50$, $N_R = 40$, $\rho_0 = 5$, $A_i = 0.99$, $B_i = 2$, $V_0 = 5.6$ and $V_1 = 2.8$. The values chosen for V_0 and V_1 are supported by [16, 17], which suggest a larger OV diffusion barrier for TiO_x (up to 2.5 eV) with respect to LCMO manganite (1.3 eV).

Figures 4(a) shows the calculated dynamic I - V curves, while figure 3(b) shows the OV profiles obtained for both HR and LR states after voltage cycling. Despite the similitude with the experimental curves, figure 4(a) shows that in the simulated I - V , the hysteresis starts immediately after the application of external voltage, indicating the onset of OV migration process. On the contrary, the experimental I - V (figure 2(a)) shows a flat region for low voltage and the hysteresis is triggered after ~ 0.5 V for positive stimulus (the hysteresis for negative stimulus is not evident in figure 2(a) as we stopped the measurements after the CC is triggered during the SET process).

This implies a delay in the onset of OV migration and indicates that an additional ingredient should be taken into account in the modeling. A clue can be obtained from the inset of figure 4(a), which shows the experimental I - V for low stimuli, below the hysteretic region, resembling the typical shape observed for a Zener diode. This suggests that due to the n and p -type character of TiO_x and LCMO_{3-x} , respectively, a n - p junction is formed at the interface between both oxides. We stress that for both $\text{Ti}/\text{PCMO}/\text{SRO}$ [7] and $\text{Al}/\text{PCMO}/\text{CMO}$ [18] systems a non-linear current-voltage behavior was reported, but the presence of diodes at $\text{MO}_x/\text{manganite}$ (M:metal) interfaces was not proposed in any case. To cope with this electronic effect in the I - V simulation, we now consider that the total voltage V along the sample is dropped as $V = \Delta V_{R(\text{OV})} + \Delta V_D$, where $\Delta V_{R(\text{OV})}$ accounts for the (resistive) voltage drop related to the redistribution of OV (equations (1)–(3)) and ΔV_D for the electronic effect at the interface and linked to the current I through the Shockley equation [19]. By taken this modification into account, we replace $V \Rightarrow \Delta V_{R(\text{OV})}$ in equation (5) and obtain the simulated I - V curve shown in figure 4(b), which now matches nicely the experimental one. The calculated HSLs are shown in figure 4(c) (main panel and inset) for different negative voltage excursions (corresponding to different CCs in the experimental counterparts), which display shapes that resemble the experimental loops (figure 2). It can be stated that the OV migration is only activated after the diode is forwardly polarized (positive voltage) or inversely polarized above breakdown (negative voltage). Further information about the diode can be obtained from

figure 4(d), which shows I - V curves at different temperatures measured in the negative quadrant. It is found that the breakdown voltage V_b (which is concomitant with the HR \rightarrow LR transition) decreases as the temperature is increased, at a rate of -2 mV K^{-1} . The evolution of V_b versus T is depicted in the inset of figure 4. The observed behavior is consistent with a low-breakdown-voltage Zener diode, characteristic of highly doped p - n junctions with a thin depletion layer [20].

Finally, we point out that the TiO_x layer displays the dominant contribution to the overall resistance of our devices. We estimated the contribution of both TiO_x and $La_{0.33}Ca_{0.67}MnO_{3-x}$ layers from equation (3) for the pristine (PR), HR and LR states, finding that the TiO_x layer displays average values of 0.1, 1.4 and 0.32 a.u./site, respectively, while the corresponding values for the $La_{1/3}Ca_{2/3}MnO_{3-x}$ layer are 0.02, 0.66 and 0.13 a.u./site, respectively. A similar scenario is proposed for TiO_x in $Ti/TiO_x/PCMO$ [7] and AlO_x in $Al/AlO_x/LSMO$ [21]. We notice that if we modify the simulation parameters to allow the $LCMO_{3-x}$ layer to dominate the resistance of the device, the calculated HSLs do not mimic the experimental ones (not shown here), reinforcing the consistency of our modeling. In relation to the bulk $LCMO$ contribution to the resistance, it is well established that this zone presents a substantial lower resistance than the interfacial $LCMO_{3-x}$ zone, due to the presence of interfacial potential barriers [5]. From this analysis, we can conclude that the contributions to the overall resistance of TiO_x , interfacial $LCMO_{3-x}$ and bulk $LCMO$ layers order according to $R_{TiO_x} > R_{LCMO_{3-x}} \gg R_{LCMO}$.

In summary we have fabricated memristive microdevices in which the RS is associated to a redox process at the $TiO_x/La_{1/3}Ca_{2/3}MnO_{3-x}$ interface. We have demonstrated the existence of multilevel states by controlling the voltage excursion during the RESET process. This multilevel capability turns our devices interesting for the development of high density RRAM devices. By adapting the VEOV model we successfully reproduced the experimental electrical behavior, after the inclusion of a Zener-type diode at the $TiO_x/LCMO_{3-x}$ interface. Our analysis indicates that OV migration between both layers is activated after the diode is polarized either in forward mode or in reverse mode above breakdown. Our work shows that a combined rectifying (p - n diode) and memristive behavior can be found at a single interface ($LCMO_{3-x}/TiO_x$), suggesting an avenue for the development of 1S1R crossbar arrays where the selecting and memristive functionalities are linked to the same interface, simplifying the device fabrication procedure. We estimated for our devices a non-linearity factor $\alpha = \frac{R_{LRS}V_{read}/2}{R_{LRS}V_{read}} \sim 10$ for $V_{read} = 0.8$ V. From the obtained α , and following the work of Huang et al [22], a 1S1R crossbar array density of some kbits can be roughly estimated for our devices. This density is lower than the 10 Mbits estimated for the high performance Ni/TiO₂/Ni/HfO₂/Pt stacks reported by Huang et al, where, unlike our case, different selecting and memristive elements were stacked (Ni/TiO₂/Ni and Ni/HfO₂/Pt, respectively) [22]. However, as the physical mechanisms reported here for $LCMO/TiO_x$ can

be expected for other p -type oxide/ TiO_x interfaces (including CMOS compatible p -type oxides), we understand there is room for materials optimization and engineering in order to significantly increase the diode nonlinearity factor and therefore the crossbar array density.

Acknowledgments

We acknowledge financial support from ANPCyT (projects PICT 0788-2013, PICT 2116-2014 and PICT 1382-2014), CONICET (project PIP 11220150100218), U N Cuyo (project 06/C455) and NanoPymes MINCYT program. We thank U Lüders and J Lecourt, from CRISMAT, for the preparation of the manganite target, and L Hueso, from nanoGUNE, for the access to their nanofabrication facilities. We also thank P Levy for the management of the NanoPymes program and N Ghenzi for his assistance during the preliminary electrical measurements.

ORCID iDs

M J Sánchez  <https://orcid.org/0000-0002-0382-8263>

References

- [1] Sawa A 2008 *Mater. Today* **11** 28
- [2] Waser R, Dittmann R, Staikov G and Szot K 2009 *Adv. Mater.* **21** 2632
- [3] Liu S Q, Wu N J and Ignatiev A 2000 *Appl. Phys. Lett.* **76** 2749
- [4] Rozenberg M J, Inoue I H and Sánchez M J 2004 *Phys. Rev. Lett.* **92** 178302
- [5] Rozenberg M J, Sánchez M J, Weht R, Acha C, Gomez-Marlasca F and Levy P 2010 *Phys. Rev. B* **81** 115101
- [6] Rubi D, Tesler F, Alposta I, Kalstein A, Ghenzi N, Gomez-Marlasca F, Rozenberg M and Levy P 2013 *App. Phys. Lett.* **103** 163506
- [7] Herpers A, Lenser C, Park C, Offi F, Borgatti F, Panaccione G, Menzel S, Waser R and Dittmann R 2014 *Adv. Mater.* **26** 2730
- [8] Asanuma S et al 2009 *Phys. Rev. B* **80** 235113
- [9] Tian B et al 2017 *Phys. Chem. Chem. Phys.* **19** 16960
- [10] Román Acevedo W et al 2017 *Appl. Phys. Lett.* **110** 053501
- [11] Ghenzi N et al 2013 *J. Phys. D: Appl. Phys.* **46** 415101
- [12] Miranda E et al 2017 *J. Appl. Phys.* **121** 205302
- [13] Asamitsu A et al 1997 *Nature* **388** 50
- [14] Herpers A 2014 Electrical characterization of manganite and titanate structures *PhD Thesis* Forschungszentrum Jülich
- [15] Hossein-Babaei F and Rahbarpour S 2011 *Solid-State Electron.* **56** 185
- [16] Wang Z-W et al 2010 *Phys. Rev. B* **82** 165309
- [17] Vengalis B et al 2001 *J. Phys. IV* **11** PR11-209
- [18] Lee H-S, Park H-H and Rozenberg M J 2015 *Nanoscale* **7** 6444
- [19] Sze S M and Ng K K 2007 *Physics of Semiconductor Devices* (Hoboken, NJ: Wiley)
- [20] Singh Tyagi M 1968 *Solid-State Electron.* **11** 117
- [21] Lee N, Lansac Y B, Hwang H C and Jang Y H 2015 *RSC Adv.* **5** 102772
- [22] Huang X et al 2011 *Electron Devices Meeting* (<https://doi.org/10.1109/IEDM.2011.6131653>)